Biophysical Journal (2010) vol. 98 (2) pp. 339-349

Triplet Imaging of Oxygen Consumption During the Contraction of a Single Smooth Muscle Cell (A7r5)

Matthias Geissbuehler[1*], Thiemo Spielmann[*†], Aurélie Formey[‡], Iwan Märki[*], Marcel Leutenegger[*§], Boris Hinz[¶], Kai Johnsson[‖], Dimitri Van De Ville[**††] and Theo Lasser[*]

[1] Corresponding author: matthias.geissbuehler@epfl.ch
Address: EPFL STI IMT LOB, BM 5.138 - Station 17,
Lausanne, CH-1015, Switzerland – Tel.: +41 21 693 77 70, Fax: +41 21 693 78 20

[*] Laboratoire d'Optique Biomédicale LOB, École Polytechnique Fédérale de Lausanne (EPFL), CH-1015 Lausanne, Switzerland

[†] Experimental Biomolecular Physics, Department of Applied Physics, Royal Institute of Technology, AlbaNova University Center, SE - 106 91 Stockholm, Sweden

[‡] Laboratory of Cell Biophysics LCB, École Polytechnique Fédérale de Lausanne (EPFL), CH-1015 Lausanne, Switzerland

[§] Department of NanoBiophotonics, Max Planck Institute for Biophysical Chemistry, D-37077 Göttingen, Germany

[¶] Laboratory of Tissue Repair and Regeneration, CIHR Group in Matrix Dynamics, Faculty of Dentistry, University of Toronto, Toronto ON M5S 3E2, Canada

[‖] Laboratory of Protein Engineering LIP1, École Polytechnique Fédérale de Lausanne (EPFL), CH-1015 Lausanne, Switzerland

[**] Medical Image Processing Laboratory MIP, École Polytechnique Fédérale de Lausanne (EPFL), CH-1015 Lausanne, Switzerland

[††] Medical Image Processing Laboratory MIP, University of Geneva, CH-1211 Geneva, Switzerland

Abstract

The measurement of tissue and cell oxygenation is important in order to understand cell metabolism. We have addressed this problem with a novel optical technique called triplet imaging that exploits oxygen induced triplet lifetime changes and that is compatible with a variety of fluorophores. A modulated excitation of varying pulse widths allows the extraction of the lifetime of the essentially dark triplet state using the high fluorescence signal intensity. This enables the monitoring of fast kinetics of oxygen concentration in living cells combined with high temporal and spatial resolution. First, the oxygen dependent triplet state quenching of tetramethylrhodamine (TMR) is first validated and calibrated in an L-ascorbic acid titration experiment demonstrating the linear relation between triplet lifetime and oxygen concentration according to the Stern-Volmer equation. Second, the method is applied to a biological cell system, employing as reporter a cytosolic fusion protein of β-galactosidase with SNAP-tag labeled with TMR. Oxygen consumption in single smooth muscle cells A7r5 during an [Arg^8]-vasopressin (AVP) induced contraction is measured. The results indicate a consumption leading to an intracellular oxygen concentration that decays mono-exponentially with time. The proposed method has the potential to become a new tool for investigating oxygen metabolism at the single cell and sub-cellular level.

Key words: fluorescence microscopy; triplet state lifetime; Modulated Excitation; tetramethylrhodamine; Transient State Imaging; oxygen concentration

Introduction

Oxygen is a key molecule involved in almost every energy cycle within a cell (1) and is responsible for regulating signalling pathways. Measurement techniques addressing partial oxygen pressure pO_2 or even directly the concentration of oxygen $[O_2]$ in vivo are of great interest because they provide us with information for deeper and more complete understanding of cell metabolism (2).

Many methods exist for local oxygen sensing at the cell level. In 1972 Knopp and co-workers attempted to demonstrate intracellular oxygen levels using fluorescence intensity quenching. However, it was only 15 years later, that a technique emerged to overcome the previous limitations and lead to more reliable measurements by using lifetime quenching of various phosphorescence emitting probes (3, 4). Meanwhile, many probes based on luminescence and phosphorescence quenching have been proposed (5–9). A newer approach towards highly localized sensing has been proposed by Finikova in 2008 by using two-photon excited phosphorescence probes (10, 11). Alternatively Koo et al. (12) proposed insertion of specifically engineered PEBBLE (probes encapsulated by biologically localized embedding) with a diameter of 120nm into the cells resulting in highly sensitive and specific nanosensors for dissolved oxygen based on phosphorescence quenching. Alternative probes for dissolved oxygen measurements include colorimetric probes (13), methods based on fluorescence lifetime measurements of the very long-living fluorophore RTDP (14, 15) and endogenous protoporphyrin IX probes that emit a characteristic delayed fluorescence signal (16, 17). The latter has been employed recently *in vivo* to measure the mitochondrial oxygen tension of the heart bringing this non-invasive technique closer to clinical application (18).

However, most of these techniques are based on low-intensity signals which make it difficult to simultaneously achieve high spatial resolution at the cellular level and high-speed to monitor oxygen kinetics. They either allow non-localized ensemble measurements or spatially resolved time-averaged signals. We present a spatio-temporally resolved oxygen measurement at the single cell level based on a fluorescence signal. The method is compatible with almost any fluorophore having a (non-radiative) triplet state that is quenched by diffusing oxygen. The method can be used with many of the different labeling protocols available.

Our experimental concept is based on a modulated excitation leading to a variation of their triplet state population. The method has been initially validated and published as a spectroscopic method by Sandén et al. (19). Recently, the same team showed the first images based on triplet lifetimes taken with a laser scanning microscope (20). Although this approach is easy to implement, the method is still limited due to long acquisition times; i.e., approximately 3 min are required to make a single image recording. Here we present a wide-field approach that allows triplet lifetime acquisition within 2 seconds, which is well suited for monitoring oxygen metabolism cycles in living cells which typically span some seconds.

In a calibration experiment, the method's ability to monitor changes in oxygen concentration with the standard fluorophore tetramethylrhodamine (TMR) was demonstrated. We employed L-ascorbic acid to remove dissolved oxygen in discrete steps while monitoring the triplet lifetime.

The technique was then applied to measure the oxygen consumption of a smooth muscle cell upon induced contraction. Previous studies on oxygen consumption by Hogan et al. used phosphorescence lifetime analysis by which the oxygen kinetics at a tissue level were determined during the contraction of muscle fibers of Xenopus laevis (21, 22). The same group also *indirectly* measured oxygen uptake kinetics at the cell level by employing a sealed chamber and measuring the extracellular oxygen concentration (23). In contrast to this earlier work on oxygen kinetics employing extra-cellular phosphorescence lifetime measurements in a sealed chamber, our method provides spatio-temporal resolution at the intra-cellular and sub-cellular level.

In accordance with these previously measured kinetics, we found that the oxygen concentrations decay mono-exponentially with time upon induced contractions.

Materials and Methods

The concept: Modulated excitation

Most fluorophores can be modeled as a three-level system, as indicated in the Jablonski scheme, with two singlet states and one triplet state (Fig. 1 *A*). The lifetime of the triplet state τ_T is typically two to four orders of magnitude longer than the lifetime of the associated excited singlet state τ_{10}. A pulsed excitation of fluorescent molecules with long-lived triplet states leads to a characteristic response of their fluorescence emission as a function of the pulse width.

The rate equations for this simplified model are:

$$\frac{\mathrm{d}}{\mathrm{d}t}\begin{bmatrix} P_0 \\ P_1 \\ P_T \end{bmatrix} = \begin{bmatrix} \frac{P_1}{\tau_{10}} + \frac{P_T}{\tau_T} - \frac{P_0}{\tau_{ex}} \\ -\frac{P_1}{\tau_{10}} - \frac{P_1}{\tau_{isc}} + \frac{P_0}{\tau_{ex}} \\ \frac{P_1}{\tau_{isc}} - \frac{P_T}{\tau_T} \end{bmatrix} \tag{1}$$

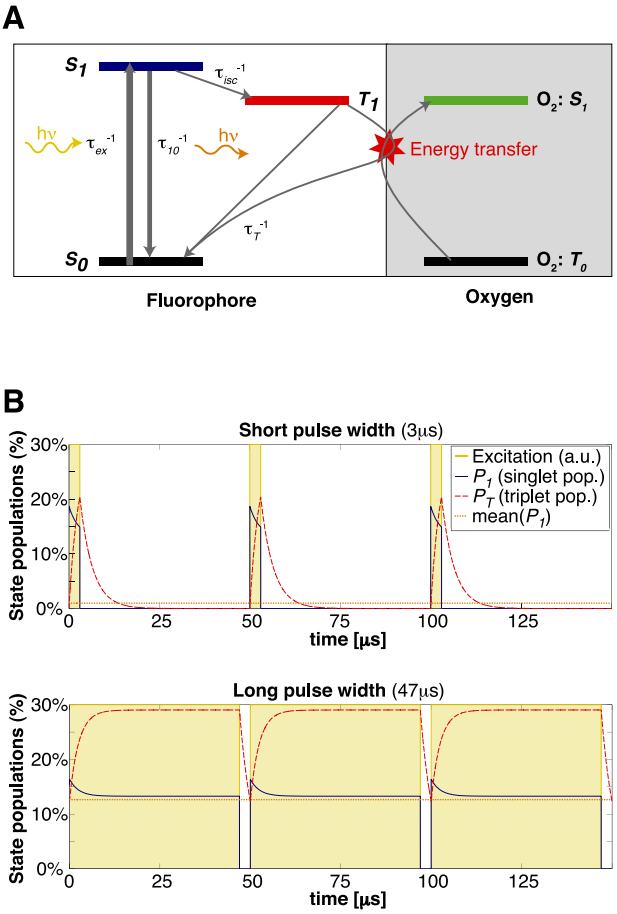

Figure 1: (*A*) Jablonski diagram of a simplified three-level model of a fluorophore, illustrating the possibility of an energy transfer from the triplet state to oxygen. (*B*) Simulation: Steady state simulations of energetic populations of a fluorescent molecule excited by rectangular pulses of 3 μs and 47μs width and 50 μs period. Typical values for TMR were used: $\tau_s = \left(\tau_{10}^{-1} + \tau_{isc}^{-1}\right)^{-1} = 2.3$ ns, $\tau_T = 3.5$ μs, $q_T = \tau_s/\tau_{isc} = 0.0014$, $\tau_{ex} = 10$ ns.

where P_0, P_1 and P_T are the respective populations of the singlet states and the triplet state, τ_{10} is the lifetime for the singlet state relaxation, τ_{isc} is the intersystem crossing lifetime from the excited singlet state to the triplet state, τ_{ex} is the excitation lifetime and τ_T is the triplet state lifetime. Based on these equations, we can simulate the response to a modulated excitation (see Fig. 1 *B*) using typical rate constants of a given fluorophore. The result of the simulation shows an increase of the triplet state population for longer pulse widths, which decreases the number of molecules available for the singlet states. This leads to a correspondingly weaker fluorescence signal for longer pulse widths compared with short excitation pulses as shown in Fig. 2 *A*.

The above result further indicates that modulated excitation can be employed to specifically improve the signal intensity. This principle is used in the triplet relaxation (T-rex) modality proposed by Donnert et al. (24, 25).

In order to increase the contrast of the kinetics-related variations and to avoid the need for a high dynamic range, we remove the strong linear increase of this signal by illuminating with an iso-dosis of light exposure for all different pulse patterns. This is achieved by varying the number of pulses (see illustrations inside Fig. 2). The resulting response for the average fluorescence intensity (Fig. 2 *B*) can be derived from Eq.1 using $(1/\tau_{10} + 1/\tau_{isc}) \approx 1/\tau_{10}$; the evolution of the triplet state population P_T is described by a second order differential equation:

$$\tau_{10}\tau_T \frac{\mathrm{d}^2 P_T}{\mathrm{d}t^2} + \left(\tau_{10} + \tau_T + \frac{\tau_{10}\tau_T}{\tau_{ex}}\right)\frac{\mathrm{d}P_T}{\mathrm{d}t} + \left(1 + \frac{\tau_{10}}{\tau_{ex}} + \frac{q_T\tau_T}{\tau_{ex}}\right)P_T = q_T\tau_T\frac{1}{\tau_{ex}} \tag{2}$$

Assuming a rectangular excitation separated into an *on* and an *off* period, allows the equation to be solved for the respective states using an onset (ansatz) of the form

$$P_T = a\exp(kt) + b \tag{3}$$

The boundary conditions are determined by the steady state assumption (eg. continuous pulses). This leads to the following expression for the average fluorescence intensity for an iso-dosis of light exposure:

$$\bar{I}_f(\vec{r}) = \gamma(\vec{r})\left(1 - \frac{\tau_T P_T^{eq}\left(1-\exp\left(-\frac{(T_p-t_p)}{\tau_T}\right)\right)}{1-\exp\left(-\frac{(T_p-t_p)}{\tau_T}+k_2 t_p\right)} \times \frac{\left(\exp\left(k_2 t_p\right)-1\right)}{t_p}\right) \tag{4}$$

where k_2 describes the population rate of the triplet state after onset of excitation, P_T^{eq} is the relative triplet state population at equilibrium for constant excitation and $\gamma(\vec{r})$ is a scaling factor depending on the concentration of fluorophores and the detection efficiency; they are given as:

$$\begin{aligned} k_2 &= -\left(\frac{\tau_{ex}+\tau_{10}+q_T\tau_T}{\tau_T(\tau_{ex}+\tau_{10})}\right) \\ P_T^{eq} &= \frac{q_T\tau_T}{\tau_{ex}+\tau_{10}+q_T\tau_T} \\ \gamma(\vec{r}) &= \eta\Gamma(\vec{r})\frac{q_f}{\tau_{ex}+\tau_{10}+q_T\tau_T} \end{aligned}$$

where t_p denotes the pulse width, T_p the repetition rate and τ_{10}, τ_T and τ_{ex} express the respective

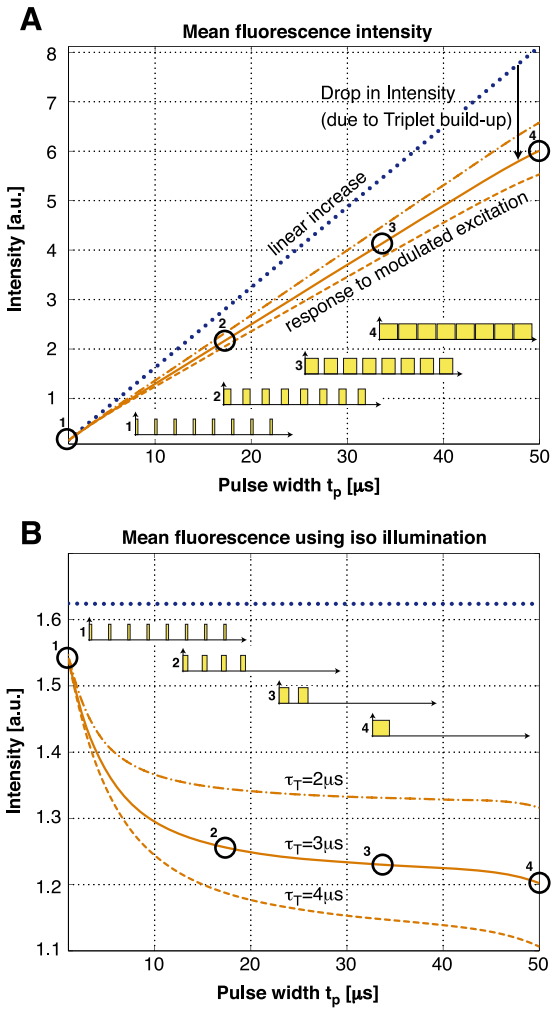

Figure 2: Simulation: (*A*) Typical fluorescence signal for different pulse widths at 50 μs repetition rate. The drop in intensity compared with the linear increase originates from an increased average triplet state population. This limits the molecules available in the singlet states and therefore decreases the fluorescent signal. (*B*) The same system illuminated with an iso-dosis of light exposure for all different pulse patterns as illustrated next to the curves.

lifetimes as used in equation (1); further, $\Gamma(\vec{r})$ is the local concentration of fluorophores, η is a conversion factor between the emitted intensity and the digital readout of the camera, $q_f = \frac{\tau_{10}^{-1}}{\tau_{10}^{-1}+\tau_{isc}^{-1}}$ is the quantum efficiency of the fluorophores and the triplet quantum yield is given by $q_T = \frac{\tau_{10}}{\tau_{isc}}$.

Oxygen

The diradical oxygen molecule exhibits the special property of having the triplet configuration as the lowest energy state (ground state) (26–28). This unique feature renders O_2 an important acceptor for energy transfers from the long-lived triplet state of a fluorescent molecule (Fig. 1 *A*). The concept of triplet state quenching by oxygen has been known for a long time (29) and it is exploited for measuring oxygen concentrations by phosphorescence lifetime where high oxygen concentrations lead to shorter phosphorescence lifetimes; see (3, 4, 22, 30). However, because of the low quantum yield and the slow turnover, phosphorescence leads only to low intensity signals.

For fluorescent molecules, triplet state quenching by oxygen is ambiguous. On the one hand, it helps to control the essentially dark triplet states because it induces the transition back to the ground state to allow re-excitation and emission of the molecule. On the other hand, it photosynthesizes singlet-oxygen by doing so, which is a highly reactive radical and a prominent source for photobleaching and cell photo-toxicity (31–35).

Oxygen versus triplet lifetime

The relationship between the concentration of a quencher (oxygen) and the triplet lifetime is described by the Stern-Volmer equation (36, 37):

$$\frac{\tau_{T0}}{\tau_T} = 1 + k_q \tau_{T0} [O_2] \tag{5}$$

where τ_{T0} is the triplet lifetime in the absence of the quencher and k_q is a quenching constant obtained by the Smoluchowski equation:

$$k_q = 4r\pi R(D_F + D_Q) N_A \times 10^3 \tag{6}$$

where D are the diffusion coefficients of the quencher and the fluorophore, R is the radius of interaction between quencher and fluorophore, r is the quenching efficiency and N_A is Avogadro's number.

Both constants τ_{T0} and k_q need to be known precisely in order to obtain an accurate relation between triplet lifetime τ_T and oxygen concentration $[O_2]$.

In the presence of reducing and oxidizing systems there exist alternative relaxation pathways for the triplet state as has been demonstrated by Rehm and Weller (38). In more recent work, this knowledge has been exploited for improved photostability (39, 40). Biological cells are complex systems with many different organelles and local environments, including different reducing and oxidizing systems. Further, a cell cannot be considered as a homogenous medium and hence we also expect varying diffusion constants. At present, it is not possible to determine $\tau_{T0} = \tau_{T0}(\vec{r})$ and $k_q = k_q(\vec{r})$ in

a precise manner for all different and non-stationary organelles of a cell. Therefore, we propose to limit the observation to the triplet state relaxation rate k_T, which is the inverse of the triplet lifetime:

$$k_T(\vec{r}) = \frac{1}{\tau_T(\vec{r})} = \frac{1}{\tau_{T0}(\vec{r})} + k_q(\vec{r})[O_2(\vec{r})] \tag{7}$$

Assuming that a variation in the concentration of the quencher does not influence $\tau_{T0}(\vec{r})$ nor $k_q(\vec{r})$, we may express the variation of the concentration as:

$$\frac{\mathrm{d}}{\mathrm{d}t}\left\{k_{\mathrm{T}}(\vec{r})\right\} = k_q(\vec{r})\frac{\mathrm{d}}{\mathrm{d}t}\left\{[O_2(\vec{r})]\right\} \tag{8}$$

In other words, the variation of the quencher concentration $\frac{\mathrm{d}}{\mathrm{d}t}\{[O_2]\}$ is proportional to the variation in the triplet relaxation rate $\frac{\mathrm{d}}{\mathrm{d}t}\left\{k_{\mathrm{T}}(\vec{r})\right\}$.

Triplet imaging setup

The system used for our experiments consists of a microscope (Zeiss Axiovert 200. Objective: Zeiss Plan-Neofluar 40x/0.75 Ph2) with a custom-made excitation setup (as shown in Fig. 3 *A*) integrating a Millenia Pro 10s Nd:YVO4 laser ($\lambda = 532$ nm; Newport Spectra Physics). An output power of > 7 W was required for a full-field illumination in order to reach an illumination intensity corresponding nearly to saturation of the fluorescent molecules. The beam was focused to a diameter of ≈ 175 μm in the sample plane, resulting in a maximum intensity of ≈ 0.59 mW/μm^2. Fast modulation of the laser beam was achieved by an acousto-optical modulator from Gooch&Housego (AOM M200-4B/E-LD4 with driver A341 for a rise-time of ≈ 10 ns). The pulse sequence was generated with a function generator (Agilent, 33250A 80 Mhz). Splitting and filtering of excitation and emission signals was achieved by filters from Chroma (Z532/10x, Q565LP, HQ620/100m) and the detection was done by an Andor Luca EMCCD camera.

All devices were controlled with a Matlab application enabling convenient and rapid acquisition.

Image processing

In order to extract the triplet lifetime, extensive image processing is necessary as illustrated schematically in Fig. 3 *B*.

Most importantly, the intensity decrease due to photo-bleaching needs to be clearly separated from the triplet lifetime kinetics related decrease. For this purpose we estimated bleaching by interlaced "bleaching" measurements at the shortest pulse width. The measured photo-bleaching curve (Fig. 4 *A*, green curve) was modeled by a decaying exponential and fitted using an efficient algorithm based on the Poisson noise assumption (41). The fitted decay parameters were then used to correct the modulated excitation response curve (Fig. 4 *A*, blue curve).

The next processing step was the fitting of the triplet lifetime. For this we fixed the values for the singlet lifetime τ_{10}, the intersystem crossing rate k_{isc} as well as the excitation rate $\tau_{\mathrm{ex}} = \tau_{\mathrm{ex}}(\vec{r})$. We

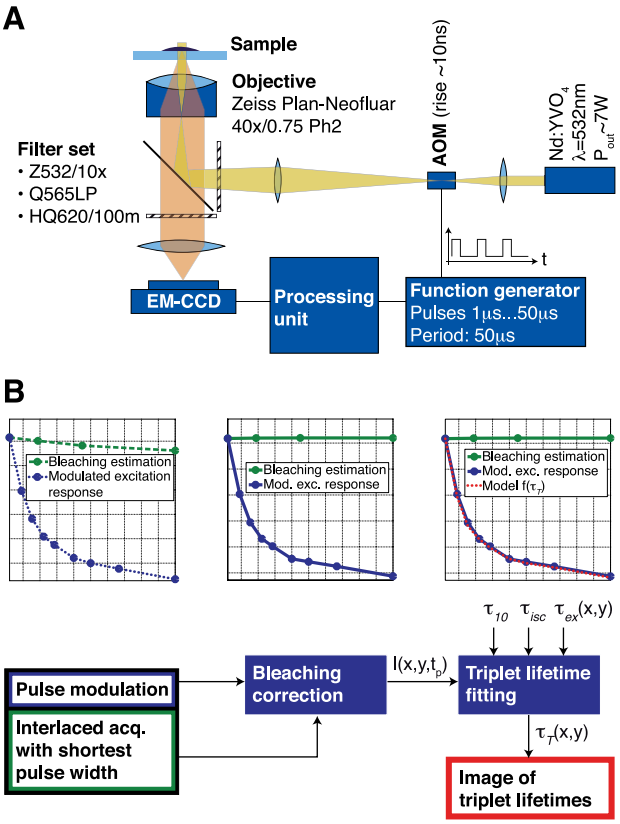

Figure 3: (*A*) Triplet state imaging setup. Beamshaping ensures a spot radius of $\approx 175\ \mu$m at the sample plane resulting in a maximum intensity of ≈ 0.6 mW/μm^2. (*B*) Image processing steps. 1 - Photo-bleaching is assessed by fitting a mono-exponential decay to the measured bleaching estimation curve. 2 - All data points are normalized to the non-bleached fraction of fluorophores. 3 - Pixel per pixel, the triplet parameters are extracted from the image stack involving prior knowledge of the lifetimes τ_{10}, τ_{isc} and $\tau_{ex}(x,y)$.

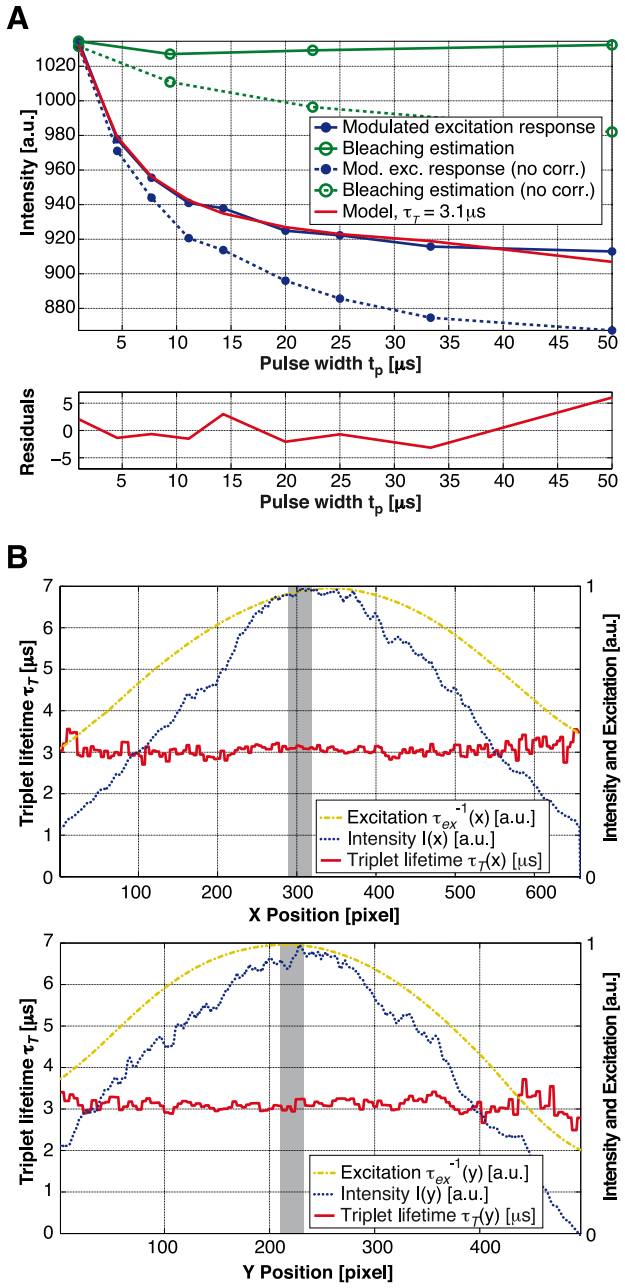

Figure 4: Observation of TMR adhering to a glass cover slide with a water droplet on top of the fluorophores. Measurement parameters: t_p = 1-50μs, T_p = 50μs, $P = 7W$, $t_{\text{ill.}}$ = 0.1ms/pulse pattern, 9 images measuring the response to a modulated excitation and 4 bleaching estimation images acquired at the shortest pulse width. (*A*) Intensity for the different pulse widths. The curves are based on a spatial average over 30x30 px in the center of the acquired images. The bleaching estimation measurement points have been plotted in order to reflect the moment they have been taken and not at their specific pulse width of 1 μs. Global fitting lead to $\tau_{\text{isc}} = 1.17$ μs. (*B*) Cross sections of the triplet lifetime fit in x and y directions (with a respective slice width and height of 30 px) in comparison with the mean fluorescence intensity over all pulse patterns as well as the fitted gaussian excitation intensity. The gray areas illustrate the region for the average that is shown in *A*.

assumed τ_{10} and k_{isc} to be constant over the whole image. For TMR, measured $\tau_{10} = 2.3$ ns on a dedicated fluorescence lifetime setup (42) with single photon counting capability (Picoquant Sepia II ps laser LDH-D-C-470; MPD PDM 50ct; Picoquant PicoHarp 300). The same fluorescence lifetime value for TMR was also measured by Eggeling et al. (43). The absorption cross section has been estimated using the absorption spectrum (Invitrogen) and a published value for TMR of $\sigma_{10}(\lambda = 515\ \mathrm{nm}) = 1.33 \times 10^{-16}\ \mathrm{cm}^2$ (43). We used an absorption cross section of $\sigma_{10}(\lambda = 532\ \mathrm{nm}) = 1.86 \times 10^{-16}\ \mathrm{cm}^2$. The intersystem crossing rate for a particular experiment was estimated by a global fit of k_{isc} and τ_{T}. Since the intersystem crossing rate could vary between different biological cells, we repeated this global fit for every experiment. For improved reliability we took typically 3-5 measurements of a particular cell and k_{isc} was set to the average of these measurements for an experiment. Since the diameter of our excitation spot was smaller than the size of our image, the spatial profile of the excitation rate had to be taken into account. We assumed a gaussian illumination profile whose position and beam width were estimated using a uniform layer of TMR deposited on a cover slide and bound to it. However, fitting a gaussian profile to the measured intensity did not lead to satisfactory results for τ_{T} over the whole range of the image. Hence an iterative fit of the triplet lifetime was used to optimize the excitation beam profile parameters in order to obtain a homogeneous triplet lifetime, as one would expect in such an experiment. Fig. 4 *B* shows the respective cross sections of the assumed excitation shape in comparison with the measured intensity profile. In order to determine not only the shape but also the value of the excitation rate, we measured the optical power transmitted through our system and calculated the maximum excitation rate at the center of the excitation spot. Therefore, the triplet imaging fit was reduced to finding two parameters for each individual pixel: the triplet lifetime τ_{T} and the factor γ, which is proportional to the intensity of a specific region. Fitting these two (non-linear) parameters by a standard optimization technique like the Marquardt-Levenberg algorithm is very slow and hence not suitable for processing an acquisition of 9 images containing 496x658 pixels. We circumvented this time consuming step and used an alternating least-squares approach for fast fitting. This resulted in typical fitting times of approximately 90 s for 152x115x9 pixels on a standard desktop computer (Intel Xeon 3.2 GHz, 2 GB RAM).

For the cell images we performed an averaging of the triplet lifetimes of three sequentially recorded measurements (2 s per measurement) in order to improve the measurement quality. The triplet relaxation values $\overline{k}_{\mathrm{T},i}$ shown in the temporal evolution of the contraction experiments, correspond to the mean values of three consecutive measurements ($k_{\mathrm{T},j}$ to $k_{\mathrm{T},j+2}$):

$$\overline{k}_{\mathrm{T},i} = \overline{k}_{\mathrm{T},i+1} = \overline{k}_{\mathrm{T},i+2} = 1/3 \times \sum_{j=i}^{i+2} k_{\mathrm{T},j}\Big|_{i=1:3:(N-2)} \tag{9}$$

The standard deviations indicated for these measurements correspond to the mean standard deviations calculated over all measurements subtracted by these respective mean values:

$$s = \left(\frac{1}{N-1} \sum_{i=1}^{N} (k_{\mathrm{T},j} - \overline{k}_{\mathrm{T},j})^2 \right)^{1/2} \tag{10}$$

Model system for calibration

Adhesion of TMR (5-(and-6)-carboxytetramethylrhodamine, succinimidyl ester (5(6)-TAMRA, SE), Invitrogen) on a glass cover-slide has been done by using bovine serum albumin (BSA) as intermediate linker between the glass cover-slide and the TMR-molecules: after deposition of a droplet of BSA on a glass cover slide, the slide was washed with 3 ml deionized water. In a second step a droplet

of TMR was applied. After 1 minute the solution was washed with 5 ml deionized water. These test samples were covered with water during the measurements, either with a droplet of water on top or by putting the slide inside a flow cell containing water. These samples served as a simple model for calibration of the experimental setup.

For the oxygen measurements, we used the enzyme ascorbase (Sigma-Aldrich) for catalysis of the oxidation of L-ascorbic acid (Sigma Aldrich) according to the following reaction:

$$2\ \text{L-ascorbic acid} + O_2 \rightarrow 2\ \text{L-dehydroascorbic acid} + 2H_2O \tag{11}$$

Titration of L-ascorbic acid removes oxygen from a solution in a controlled way (37). The final reaction mix consisted of 3 ml H_2O, 10 units ascorbase (1 unit oxidizes 1 μmole of L-ascorbic acid per minute), 20 mM sodium phosphate buffer and 0.05‰(w/v) bovine serum albumin (BSA). Adding 300 μl of a solution of 25.5 mM L-ascorbic acid removes all dissolved oxygen inside 3 ml of H_2O at room temperature provided that there is no re-oxygenation from the environment.

In order to minimize the oxygen uptake during the experiment, the observation was done in a custom-made PDMS-flowcell with an observation volume of ≈ 20 mm^3 connected by tubing with low gas permeability (Ismatec, Fluran HCA with inner diameter of 0.89 mm) to a peristaltic pump (Ismatec Reglo Digital) at 1.5 μl/s. The solution reservoir was placed in a larger container connected to a low continuous flow of nitrogen. The L-ascorbic acid doses were added with a syringe through a tiny access hole in the container.

This model system allowed a verification of the acquisition method and the fitting algorithm for different oxygen concentrations. As a control, we measured the oxygen concentration inside the reservoir with a Mettler Toledo oxygen probe (SG6 Seven Go Pro dissolved oxygen meter with InLab 605 sensor).

Smooth muscle cells A7r5 and TMR labeling

For biological measurements, we used the rat thoracic aorta smooth muscle cell line A7r5 (44) (Promochem; CRL-1444) cultured in Dulbecco's modified eagle medium (DMEM, GIBCO; 41965) supplemented with 10% fetal calf serum (FCS). We used two different labeling protocols: one to realize transient transfections and one for stable transfections. For the stable transfection we used A7r5 cells stably transfected with pNuc SNAP β-gal plasmids expressing a fusion protein of SNAP-tag and β-galactosidase (SNAP-β-gal); SNAP-tag fusion proteins can be specifically labeled with different fluorophores in living cells (45). Stably transfected clones expressing SNAP β-gal fusion proteins were selected by adding 2 mg/mL G418 (Geneticin disulfate salt, Sigma; G5013) to the culture medium.

For the transient transfection we used the same A7r5 cell line that we transfected according to a standard transfection protocol using the Jet Pei technique (Polyplus transfection; 101-05) with 2 μg plasmid DNA per 35 mm dish. The transient transfections were started 24-48 h before the experiment.

Two days prior to the experiments, respectively one day before the transfection, the cells were transferred into 3.5 cm microscope observation dishes (Ibidi) coated with collagen.

The day of the experiment, cells were labeled by loading the dishes for 5 minutes at room temperature with 200 μL of a solution of 1 μM TMR-Star (Covalys; LK040) in DMEM with 10% FCS. Cells where then washed three times in DMEM with 10% FCS then incubated for 5 minutes at each step

at 37 °C. Finally the cells were incubated for at least three hours until the experiment. Before measurements the medium was replaced by a Hank's Buffered Salt Solution (HBSS, GIBCO).

Cell contraction was induced using [Arg^8]-vasopressin acetate salt (Sigma; V9879) at a final concentration of 500 nM AVP. This hormone is well known to initiate a vasoconstriction of the smooth muscle cells at this concentration (46, 47).

Results

Model system: TMR on cover slide

Fig. 4 *A* shows a typical modulated excitation response and a bleaching estimation curve for a measurement of a TMR layer adhering to a glass cover slide. With the bleaching estimation, photobleaching could be taken into account accurately as shown by the corrected fluorescence responses. By global fitting we found $\tau_{\text{isc}} = 1.17\ \mu s$. The average triplet lifetime is around $\tau_T = 3.1\ \mu s$. These values are comparable to values measured for TMR in solution: $\tau_{\text{isc}} = 1.85\ \mu s$ and $\tau_T = 2.5\ \mu s$ (43). The cited values were measured with fluorescence correlation spectroscopy (FCS) and varying excitation intensity (48). The differences from our results are probably due to higher order artifacts as described in the discussion.

Triplet lifetime versus oxygen concentration

We performed calibration experiments by lowering the dissolved oxygen concentration in discrete steps by titration of L-ascorbic acid. In parallel to the triplet lifetime acquisitions, the dissolved oxygen concentration was monitored with an oxygen probe as reference. As shown in Fig. 5 *A*, the probe revealed the linear decrease in dissolved oxygen as expected in theory, which demonstrates that the titration of L-ascorbic acid is indeed proportional to the removed amount of dissolved oxygen. The graph of the triplet state relaxation rate k_T ($= 1/\tau_T$), Fig. 5 *C*, also demonstrates a linear relationship, which suggests that the molecules' response to oxygen can be described by the Stern-Volmer model. This proves that TMR as reporter molecule measured with our method works well for determining different oxygen concentrations. However, despite a minimized surface in contact with air, re-oxygenation of the sample could not be prevented totally. Due to this, the titration of 300 μl L-ascorbic-acid did not remove all oxygen in the solution. Nevertheless, the experiment allowed us to measure the response of our system in physiological conditions and it demonstrates nicely the linearity of the quenching mechanism.

Triplet lifetime inside single smooth muscle cells A7r5

To test our triplet imaging method in a biologically relevant context, we performed AVP stimulated contraction experiments with smooth muscle cells. The fluorescence signal originates from TMR linked to SNAP-tag-β-galactosidase which is a cytosolic protein linked to a tag for labeling (49).

Fig. 6 shows two typical experiments. In Fig. 6 A_2 and B_2, the color encodes the different triplet lifetimes, whereas the intensity is proportional to the fluorescence intensity. Fig. 6 A_3 and B_3 shows the temporal evolution of the triplet relaxation rate over a selected area (white square on the corre-

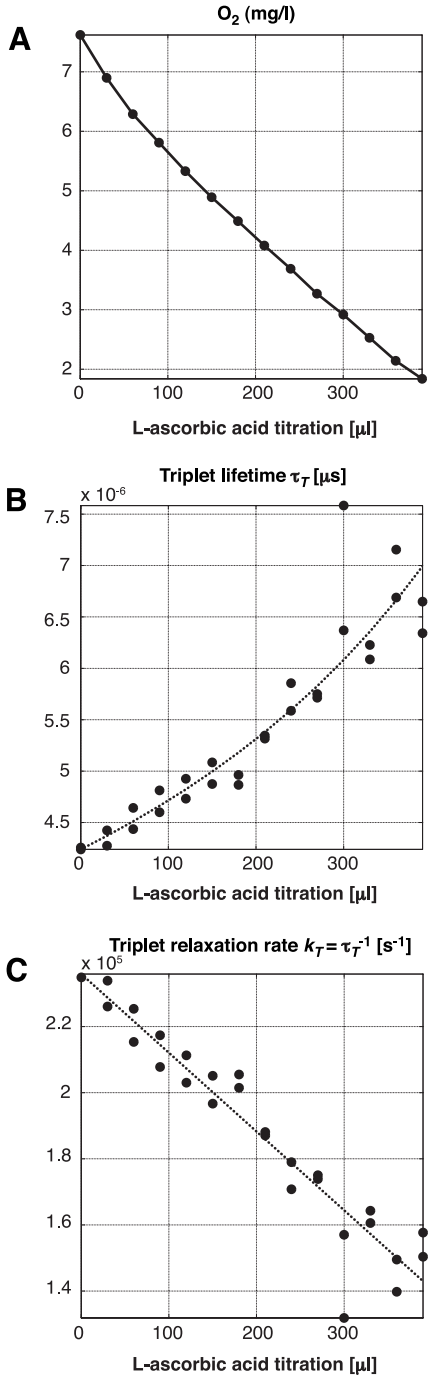

Figure 5: Observation of TMR adhering to a glass cover slide in a flow cell setup with ascorbase in solution. Titration of 25.5 mM L-Ascorbic-Acid removes the oxygen in controlled discrete steps. (*A*) Dissolved oxygen as measured by a commercial probe (Mettler Toledo). (*B*) Triplet lifetime measurement using an average intersystem crossing of $\tau_{isc} = 0.69$ μs obtained by a global fitting over 7 measurements. (*C*) Triplet state relaxation rate.

sponding images on the left side). As mentioned above the variation in $k_T = 1/\tau_T$ is proportional to the variation in the oxygen concentration. After global stimulation with 500 nM [Arg^8]-vasopressin (AVP) the cells undergo a contraction. This leads to an oxygen consumption inside the cell, which can be observed on the temporal evolution of the triplet relaxation rate. In order to achieve longer measurement times and minimal phototoxicity for the cells, we have compromised the image quality slightly by reducing the excitation power. But one can easily obtain better resolutions and higher signal quality when using higher excitation levels. Such an image is not shown here but it can be found in the supplementary material along with movies of the experiments.

The results of three measurements with global AVP stimulation are shown in Fig. 7 A_1 in comparison with two negative controls without addition of AVP. In Fig. 7 A_2 the temporal evolutions are normalized with respect to their initial and final steady states. For the negative controls we used a factor of 0.4×10^{-5} for the normalization corresponding to a typical difference between the steady state values before and after adding AVP.

The temporal evolution presented in the three curves has been observed in 84% of the observed cells (n=25). The remaining 16% of cells did not show a visible decrease in triplet relaxation rate after the addition of AVP similar to the negative control experiments (n=5).

Discussion

The L-ascorbic acid titration experiment (Fig. 5) demonstrates that the proposed method is able to determine variations in oxygen concentration. The sensitivity of this method is not as good as in other methods (4, 12, 37). However the high intensity of the fluorescence signal enables a combined performance of temporal and spatial resolution well beyond what can be achieved with methods based on phosphorescence quenching or on other mechanisms leading to low intensity signals.

Since high laser excitation power is required to increase the contrast based on the triplet state buildup, we reduced the acquisition times such that there is illumination during only 1.2 ms per acquisition of 12 images. Despite using a fairly photostable fluorophore, bleaching has been an important issue. Typically at the end of an experiment (after around 30 acquisitions of 12 images each), the fluorescence signal corresponds to about 20% of the initial intensity, limiting the total number of acquisitions that can be made on the same cell.

Nevertheless, the proposed functional imaging method was successfully applied in a study of oxygen consumption during drug-induced contraction of single smooth muscle cells (Fig. 7). In most cells we measured mono-exponentially falling intracellular oxygen concentration without initial delay upon the addition of 500 nM AVP. On average we found a typical decay constant of ≈ 40 s for these cells. These positive results can be compared to experiments where no AVP was added (Fig. 7 cells 4 and 5).

Triplet lifetime images of cells (Fig. 6 and supplemental material for a high spatial resolution image) reveal areas of long (yellow-red color code) and short triplet lifetimes with heterogeneous cellular distribution. In general, these areas indicate different oxygen concentrations as well as different local environments of the dyes. Biological cells contain various organelles and exhibit different subcellular compartments with corresponding dimensions that can locally influence the triplet state lifetime. In particular, organelles of the endosomal and lysosomal compartments are characterized by distinct pH. Large shifts in the pH will lead to noticeable changes in the triplet state of the dyes. Another explanation for these areas may be sites of mitochondria, the main oxygen-consuming organelles in a cell. This is corroborated by matching triplet lifetime images with phase contrast im-

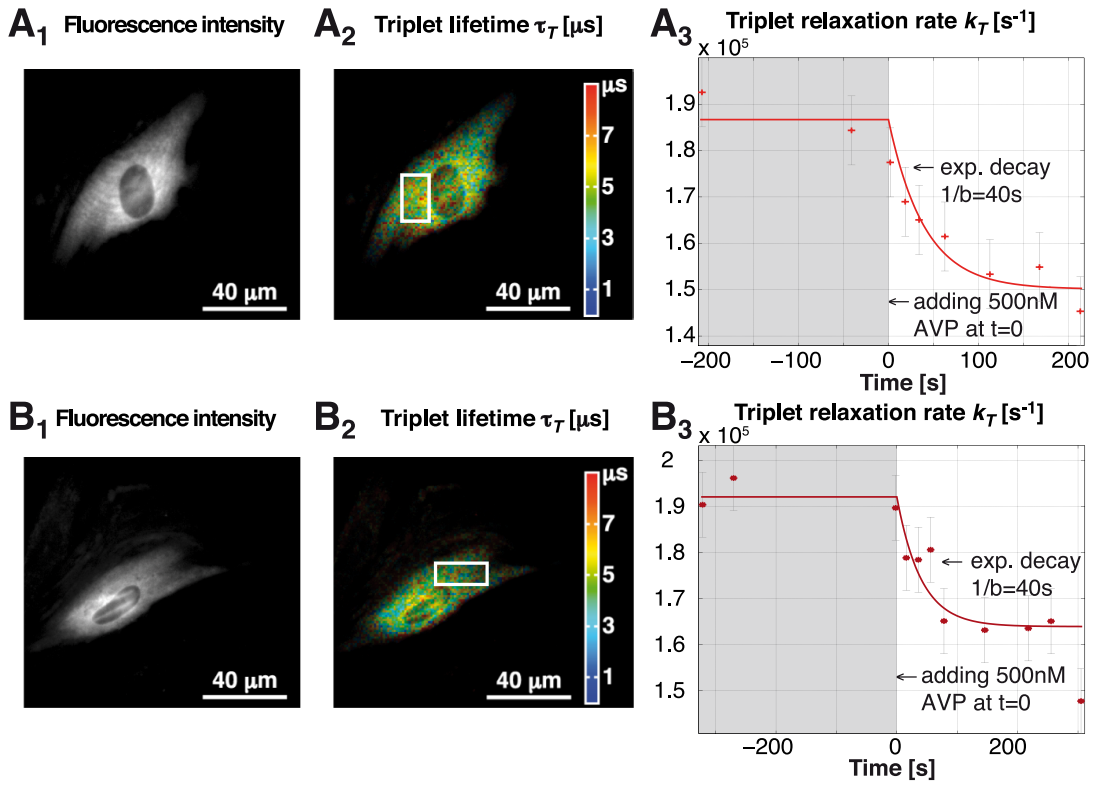

Figure 6: Two experiments on contraction of smooth muscle cells A7r5 with transient transfections of the cytosolic fusion protein β-galactosidase (SNAP-β-gal) employed for the labeling with TMR. Contraction was initiated with [Arg^8]-vasopressin (AVP). (A_2) and (B_2) Triplet lifetime image with color encoded lifetime. (A_3) and (B_3) show the temporal evolution of the average triplet relaxation rate for the region inside the white rectangle. The result indicates a variation in the oxygen concentration following a monoexponential decay (the approximate decay parameter was estimated from multiple experiments). We used for (A): $\tau_{isc} = 2.12$ μs and for (B): $\tau_{isc} = 2.01$ μs, both values were obtained by global fitting on several measurements. The image quality was optimized for multiple measurements. A typical triplet lifetime image with higher spatial resolution can be found in the supporting material.

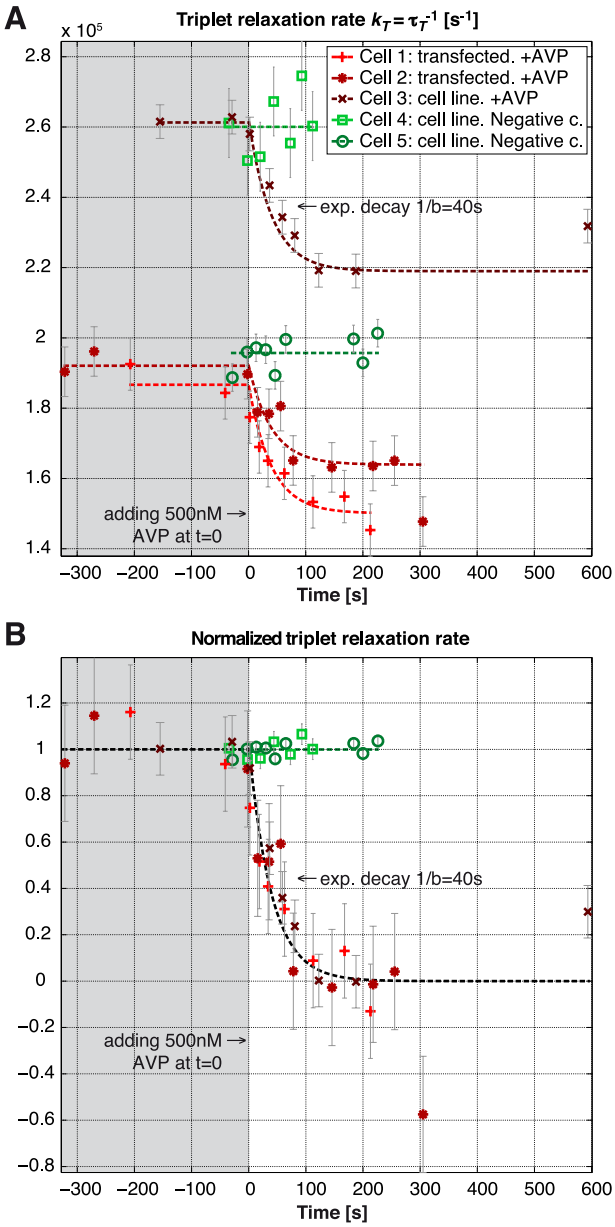

Figure 7: Three experiments on contraction of smooth muscle cells A7r5 upon addition of AVP and two negative controls where no AVP was added. (*A*) Average triplet relaxation rate measured on a small area inside the respective cells. (*B*) Relaxation rates normalized with respect to the initial and final steady state. For the negative controls we used a factor of 0.4×10^{-5} for the normalization corresponding to a typical difference between the steady state values before and after adding AVP. Global fitting was used to determine the respective intersystem crossing rates τ_{isc} leading to the following values: (Cell 1) 2.12 μs (Cell 2) 2.01 μs (Cell 3) 1.19 μs (Cell 4) 1.08 μs (Cell 5) 2.01 μs. Movies of three experiments can be found in the supporting material.

This is the final draft. DOI of official version: 10.1016/j.bpj.2009.10.006

ages, in which mitochondria appear as phase-dense circular structures with ≈ 1 μm diameter. Our data indicate that in sub-cellular areas with lower density of these structures, the corresponding triplet relaxation rate is significantly higher (see phase contrast image in movie 3, right of the nucleus). This example may indicate an intracellular oxygen gradient, created by the absence of mitochondria in this area. To this end, we can only reasonably speculate about the nature of the sub-cellular compartments coinciding with distinct triplet lifetimes. Further experiments using specific compartmental marker proteins will be needed to clarify their nature.

We observed rather large differences between different cells in their triplet relaxation rate k_{T} as well as their intersystem crossing rate k_{isc}. When analyzing the deviating measurements we found differences in the bleaching correction in contrast to experiments that lead to $k_{\mathrm{isc}} \approx 2$ μs. The deviating correction leads to a systematic small hump on the corrected modulated excitation response for pulse widths around 15 μs (as also visible in Fig. 4 *A*). This probably accounts for the higher intersystem crossing rates (and lower triplet lifetimes). We think the effect stems from higher order energy states that start to be populated for longer excitation pulses ($t_p > 10$ μs). This would lead to an additional kinetic response upon modulated excitation which we have not taken into account in the current three state model. Correcting for this higher order effect would require a more advanced bleaching estimate measurement which is beyond the scope of this paper.

As described above, there was an important decrease in fluorescence intensity over a full experiment. This led to difficulties in fitting low intensity measurements at the end of the experiment and explains the deviations of the two outliers at the very end of the measurement of cell 2 and 3. Hence the standard deviation as described in “materials and methods" is actually expected to grow with measurement time although the measurements themselves do not indicate it.

Our measurements demonstrate that the proposed method is well suited to address biological questions related to fast oxygen kinetics at the cellular and sub-cellular level. Our results are in accordance with previously reported measurements of oxygen consumption during contraction of skeletal muscle fibers of Xenopus laevis (21) as well as with indirect measurements of the oxygen uptake of single cells in a sealed chamber (23).

The method could be further refined by taking care of variations of the intersystem crossing rate k_{isc} during the experiment. Such effects could be caused by variations of the singlet oxygen concentrations. In some cases with strong labeling (eg. when labeling the cells with nuclear localized proteins) we did indeed see continuous variations of the intersystem crossing rate during the experiment that might have been due to increased photosensitized singlet oxygen. Taking into account higher triplet states might improve the parameter extraction but at the expense of a far more complicated fitting procedure and the potential risk of leading to a less robust fitting.

Conclusion

We have outlined a novel concept for functional wide-field microscopy which is able to image the triplet kinetics of fluorescent probes. Using a rapidly modulated excitation and a slow camera, spatio-temporal variations of the triplet state kinetics of many standard fluorophores can be assessed.

Firstly, we validated our concept on thin TMR films deposited on microscope cover slips. An oxygen depletion experiment resulted in a proportional decrease of the measured triplet relaxation rate k_T ($= 1/\tau_T$) as predicted by the well known Stern-Volmer equation. Secondly, measurements of the oxygen consumption of single smooth muscle cells A7r5 showed a mono-exponential decay of the

intracellular oxygen concentration upon stimulated contraction. The decay started without measurable delay and had a characteristic decay time of 40 s, which is in good agreement with measured oxygen consumption in skeletal muscle fibers reported by Hogan et al. (21).

In our opinion, the proposed triplet state imaging concept is a valid tool for investigating the inter- and intracellular oxygen concentration variations in live cells or small tissue fragments. It is particularly attractive because it is able to image the metabolism of live cells with a time resolution in the order of a second at a state-of-the-art spatial resolution and field of view.

This work was funded by the European Commission within the sixth research framework program.

References

1. Chandel, N., and G. Budinger, 2007. The cellular basis for diverse responses to oxygen. *Free Radical Biology and Medicine* 42:165–174.

2. Springett, R., and H. Swartz, 2007. Measurements of oxygen in vivo: Overview and perspectives on methods to measure oxygen within cells and tissues. *Antioxidants and Redox Signaling* 9:1295–1301.

3. Rumsey, W., J. Vanderkooi, and D. Wilson, 1988. Imaging of phosphorescence: A novel method for measuring oxygen distribution in perfused tissue. *Science* 241:1649–1651.

4. Vanderkooi, J., G. Maniara, T. Green, and D. Wilson, 1987. An optical method for measurement of dioxygen concentration based upon quenching of phosphorescence. *Journal of Biological Chemistry* 262:5476–5482.

5. Xu, W., 1994. Oxygen sensors based on luminescence quenching: Interactions of metal complexes with the polymer supports. *Anal Chem* 66:4133–4141.

6. Hartmann, P., M. Leiner, and M. Lippitsch, 1995. Luminescence quenching behavior of an oxygen sensor based on a Ru(II) complex dissolved in polystyrene. *Anal Chem* 67:88–93.

7. Demas, J., B. DeGraff, and P. Coleman, 1999. Oxygen sensors based on luminescence quenching. *Anal Chem* 71:793A–800A.

8. Papkovsky, D. B., 1995. New oxygen sensors and their application to biosensing. *Sensors and Actuators, B: Chemical* B29:213–218.

9. Vanderkooi, J., W. Wright, and M. Erecinska, 1990. Oxygen gradients in mitochondria examined with delayed luminescence from excited-state triplet probes. *Biochemistry* 29:5332–5338.

10. Finikova, O., P. Chen, Z. Ou, K. Kadish, and S. Vinogradov, 2008. Dynamic quenching of porphyrin triplet states by two-photon absorbing dyes: Towards two-photon-enhanced oxygen nanosensors. *Journal of Photochemistry and Photobiology A: Chemistry* 198:75–84.

11. Finikova, O., A. Lebedev, A. Aprelev, T. Troxler, F. Gao, C. Garnacho, S. Muro, R. Hochstrasser, and S. Vinogradov, 2008. Oxygen microscopy by two-photon-excited phosphorescence. *ChemPhysChem* 9:1673–1679.

12. Koo, Y.-E., Y. Cao, R. Kopelman, S. Koo, M. Brasuel, and M. Philbert, 2004. Real-Time Measurements of Dissolved Oxygen Inside Live Cells by Organically Modified Silicate Fluorescent Nanosensors. *Anal Chem* 76:2498–2505.

13. Evans, R., P. Douglas, J. Williams, and D. Rochester, 2006. A novel luminescence-based colorimetric oxygen sensor with a "traffic light" response. *Journal of Fluorescence* 16:201–206.

14. Gerritsen, H., R. Sanders, A. Draaijer, C. Ince, and Y. Levine, 1997. Fluorescence lifetime imaging of oxygen in living cells. *Journal of Fluorescence* 7:11–15.

15. Sud, D., and M.-A. Mycek, 2009. Calibration and validation of an optical sensor for intracellular oxygen measurements. *Journal of Biomedical Optics* 14:020506.

16. Mik, E., J. Stap, M. Sinaasappel, J. Beek, J. Aten, T. van Leeuwen, and C. Ince, 2006. Mitochondrial PO2 measured by delayed fluorescence of endogenous protoporphyrin IX. *Nature Methods* 3:939–945.

17. Mik, E., T. Johannes, C. Zuurbier, A. Heinen, J. Houben-Weerts, G. Balestra, J. Stap, J. Beek, and C. Ince, 2008. In vivo mitochondrial oxygen tension measured by a delayed fluorescence lifetime technique. *Biophysical Journal* 95:3977–3990.

18. Mik, E., C. Ince, O. Eerbeek, A. Heinen, J. Stap, B. Hooibrink, C. Schumacher, G. Balestra, T. Johannes, J. Beek, A. Nieuwenhuis, P. van Horssen, J. Spaan, and C. Zuurbier, 2009. Mitochondrial oxygen tension within the heart. *Journal of Molecular and Cellular Cardiology* 46:943–951.

19. Sandén, T., G. Persson, P. Thyberg, H. Blom, and J. Widengren, 2007. Monitoring kinetics of highly environment sensitive states of fluorescent molecules by modulated excitation and time-averaged fluorescence intensity recording. *Anal Chem* 79:3330–41.

20. Sandén, T., G. Persson, and J. Widengren, 2008. Transient State Imaging for Microenvironmental Monitoring by Laser Scanning Microscopy. *Anal. Chem.* 80:9589–9596.

21. Hogan, M., 2001. Fall in intracellular Po2 at the onset of contractions in Xenopus single skeletal muscle fibers. *Journal of Applied Physiology* 90:1871–1876.

22. Hogan, M., 1999. Phosphorescence quenching method for measurement of intracellular PO2 in isolated skeletal muscle fibers. *Journal of Applied Physiology* 86:720–724.

23. Kindig, C., K. Kelley, R. Howlett, C. Stary, and M. Hogan, 2003. Assessment of O2 uptake dynamics in isolated single skeletal myocytes. *Journal of Applied Physiology* 94:353–357.

24. Donnert, G., C. Eggeling, and S. Hell, 2009. Triplet-relaxation microscopy with bunched pulsed excitation. *Photochemical and Photobiological Sciences* 8:481–485.

25. Donnert, G., C. Eggeling, and S. Hell, 2007. Major signal increase in fluorescence microscopy through dark-state relaxation. *Nature Methods* 4:81–86.

26. Krasnovsky, –., 2007. Luminescence and photochemical studies of singlet oxygen photonics. *Journal of Photochemistry & Photobiology* .

27. Mulliken, R., 1932. The interpretation of band spectra part III. Electron quantum numbers and states of molecules and their atoms. *Reviews of Modern Physics* 4:1–86.

28. Kearns, D., 1971. Physical and chemical properties of singlet molecular oxygen. *Chemical Reviews* 71:395–427.

29. Kautsky, H., and G. Müller, 1947. Luminescenzumwandlung durch Sauerstoff – Nachweis geringster Sauerstoffmengen. *Z Naturforsch A* 2:167–172.

30. Vinogradov, S., and D. Wilson, 1994. Phosphorescence lifetime analysis with a quadratic programming algorithm for determining quencher distributions in heterogeneous systems. *Biophysical Journal* 67:2048–2059.

31. Mitra, S., and T. Foster, 2000. Photochemical oxygen consumption sensitized by a porphyrin phosphorescent probe in two model systems. *Biophysical Journal* 78:2597–2605.

32. Georgakoudi, I., and T. Foster, 1998. Singlet Oxygen- Versus Nonsinglet Oxygen-Mediated Mechanisms of Sensitizer Photobleaching and Their Effects on Photodynamic Dosimetry. *Photochemistry and Photobiology* 67:612–625.

33. Stracke, F., M. Heupel, and E. Thiel, 1999. Singlet molecular oxygen photosensitized by Rhodamine dyes: Correlation with photophysical properties of the sensitizers. *Journal of Photochemistry and Photobiology A: Chemistry* 126:51–58.

34. Valeur, B., 2002. Molecular Fluorescence: Principles and Applications. *Wiley-VCH* 402.

35. Hoebe, R. A., C. H. V. Oven, T. W. J. Gadella, P. B. Dhonukshe, C. J. F. V. Noorden, and E. M. M. Manders, 2007. Controlled light-exposure microscopy reduces photobleaching and phototoxicity in fluorescence live-cell imaging. *Nature Biotechnology* 25:249.

36. Stern, O., and M. Volmer, 1919. The fading time of fluorescence. *Phys Z* 20:183–188.

37. Lo, L.-W., C. Koch, and D. Wilson, 1996. Calibration of oxygen-dependent quenching of the phosphorescence of Pd-meso-tetra (4-carboxyphenyl) porphine: A phosphor with general application for measuring oxygen concentration in biological systems. *Analytical Biochemistry* 236:153–160.

38. Rehm, D., and A. Weller, 1970. Kinetics of Fluorescence Quenching by Electron and H-Atom Transfer. *Israel J Chem* 8:259–271.

39. Vogelsang, J., R. Kasper, C. Steinhauer, B. Person, M. Heilemann, M. Sauer, and P. Tinnefeld, 2008. A reducing and oxidizing system minimizes photobleaching and blinking of fluorescent dyes. *Angewandte Chemie - International Edition* 47:5465–5469.

40. Widengren, J., A. Chmyrov, C. Eggeling, P.-Å. Löfdahl, and C. Seidel, 2007. Strategies to improve photostabilities in ultrasensitive fluorescence spectroscopy. *Journal of Physical Chemistry A* 111:429–440.

41. Gatland, I. R., and W. J. Thompson, 1992. Parameter bias elimination for log-transformed data with arbitrary error characteristics. *American Journal of Physics* 61:269–272.

42. Leutenegger, M., H. Blom, J. Widengren, C. Eggeling, M. Gösch, R. Leitgeb, and T. Lasser, 2006. Dual-color total internal reflection fluorescence cross-correlation spectroscopy. *Journal of Biomedical Optics* 11.

43. Eggeling, C., J. Widengren, R. Rigler, and C. Seidel, 1998. Photobleaching of Fluorescent Dyes under Conditions Used for Single-Molecule Detection: Evidence of Two-Step Photolysis. *Anal Chem* 70:2651–2659.

44. Kimes, B., and B. Brandt, 1976. Characterization of 2 putative smooth muscle cell lines from rat thoracic aorta. *Experimental Cell Research* 98:349–366.

45. Keppler, A., S. Gendreizig, T. Gronemeyer, H. Pick, H. Vogel, and K. Johnsson, 2003. A general method for the covalent labeling of fusion proteins with small molecules in vivo. *Nature Biotechnology* 21:86–89.

46. Takeda, K., H. Meyer-Lehnert, J. Kim, and R. Schrier, 1988. AVP-induced Ca fluxes and contraction of rat glomerular mesangial cells. *American Journal of Physiology - Renal Fluid and Electrolyte Physiology* 255.

47. Renterghem, C. V., G. Romey, and M. Lazdunski, 1988. Vasopressin modulates the spontaneous electrical activity in aortic cells (line A7r5) by acting on three different types of ionic channels. *Proc Natl Acad Sci USA* 85:9365–9369.

48. Widengren, J., U. Mets, and R. Rigler, 1995. Fluorescence correlation spectroscopy of triplet states in solution: A theoretical and experimental study. *Journal of Physical Chemistry* 99:13368–13379.

49. Keppler, A., H. Pick, C. Arrivoli, H. Vogel, and K. Johnsson, 2004. Labeling of fusion proteins with synthetic fluorophores in live cells. *Proc Natl Acad Sci USA* 101:9955–9959.